






# Land subsidence mapping and monitoring using modified persistent scatterer interferometric synthetic aperture radar in Jharia Coalfield, India

SUNIL KUMAR<sup>1,\*</sup> , DHEERAJ KUMAR<sup>1</sup> , SUMIT KUMAR CHAUDHARY<sup>1</sup>,  
NARENDRA SINGH<sup>1</sup>  and KAPIL KUMAR MALIK<sup>2</sup>

<sup>1</sup>Department of Mining Engineering, Indian Institute of Technology (Indian School of Mines),  
Dhanbad 826 004, India.

<sup>2</sup>Radar System and Services, Chandigarh, India.

\*Corresponding author. e-mail: skumar.ismu@gmail.com skumar781@iitism.ac.in

MS received 4 June 2018; revised 10 February 2020; accepted 30 March 2020; published online 27 June 2020

Subsidence has been adversely affecting Jharia Coalfield (JCF) for the last few decades. This study attempts to show the feasibility of the modified Persistent Scatterer Interferometric Synthetic Aperture Radar (PS-InSAR) technique with C-band SAR data to investigate the slow surface deformation caused by coal mine fire and underground mining activities in JCF. Also, a multi-temporal analysis of SAR images of ENVISAT ASAR has been carried out for monitoring and mapping of temporal land subsidence of the area under study. The modified PSI technique has proven its ability to detect land subsidence over the vegetated and rural areas. It also resolves low spatial density of permanent scatterers by considering partially correlated scatterers as permanent scatterers (PSs) and extracting information from these PSs. The study has been concentrated towards detecting continuous slow rate subsidence of five major sites of JCF. The maximum rate of slow deformation among all sites is recorded as 29 mm/year with a cumulative subsidence value of 90 mm. Field validation of subsidence results obtained through PS-InSAR is correlated with the previously published report and the master plan of JCF, showing subsidence locations. Conclusively, the adopted methodology is practically feasible for detection, monitoring and mapping of slow deformation using C-band SAR data in coal mine area.

**Keywords.** Modified PS-InSAR; multi-temporal analysis; land subsidence; Jharia coalfield (JCF); remote sensing.

## 1. Introduction

Land subsidence is considered to be a natural-anthropogenic hazard impacting both the society and the environment. Land subsidence occurs mainly due to underground mining and subsurface coal fire. Most of the land subsidences occur due to different activities in underground mining such as overexploitation of coal, minerals, groundwater

and petroleum products, depillaring of the existing galleries and waterlogging of the abandoned galleries (Chatterjee *et al.* 2006; Jianjun *et al.* 2012). Subsidence vulnerability becomes more in those areas where large underground voids have been created by extracting coals, ores, etc. (Miao *et al.* 2008; Guang *et al.* 2009; Engelbrecht and Inggs 2013; Gupta *et al.* 2014; Paradella *et al.* 2015; Qin and Perissin 2015; Ishwar and Kumar 2017).

JCF witnesses the maximum number of surface and subsurface coal fires among all coalfields in India. Underground mining as well as subsurface coal fire are responsible for the occurrence of land subsidence in coal mining area (Chatterjee 2006; Jianjun *et al.* 2012; Shen and Poulsen 2014; Pandey *et al.* 2016). Coal seams are getting burnt due to shallow depth subsurface fire (<40 m) (Mukherjee *et al.* 1991) creating the vast void and leading to surface cracks and land subsidence (Chatterjee *et al.* 2015). Chatterjee (2006) has reported that the spatial dynamics of land subsidence may be influenced by lateral propagation of coal fire. Jharia town (approx. population of 82,000 according to the census of 2001, India) has suffered from the danger of coal fire and land subsidence due to extensive coal extraction by the mining operation and subsurface coal fire. Spatial-temporal monitoring and mapping of land subsidence with precise measurement is the need of the hour for management and control of surface deformation caused by both underground mining as well as sub-surface coal fires.

The conventional method of subsidence monitoring technique is based on ground methods which depend on precise level, auto level and digital level measuring systems. Precision leveling technique provides a high relevant measurement with sub-millimeter to millimeter accuracy. However, firstly, it is very time-consuming and labour intensive approach as compared to other space-based methods such as Global Positioning System (GPS)/Global Navigational Satellite System (GNSS) and remote sensing methods. Secondly, ground-based subsidence monitoring techniques also pose safety risks since measurements have to be taken along subsidence prone areas. GPS/GNSS time series analysis for deformation mapping proved its significance through different studies (Lü *et al.* 2008; Jing-xiang and Hong 2009; Wang *et al.* 2011; Chatterjee *et al.* 2015). However, GPS/GNSS suffers from some of the same vexing problems affecting traditional surveys. The limitations of GPS/GNSS techniques have been overcome by space-borne imaging techniques. The invention of radar interferometry elevates imaging-based subsidence monitoring techniques to a very notable position because of its capability of synoptic coverage, atmospheric conditions independence, the flexibility of any time observations, and high accuracy. The imaging techniques also reduce the safety risk and decrease the expenses that are

inherent in conventional methods due to extensive fieldwork.

Since last few decades, many research studies have been carried out globally for monitoring land subsidence induced by underground mining in various mining fields using differential interferometric SAR (D-InSAR) technique (Stow and Wright 1997; Perski 1998; Carnec and Delacourt 2000; Strozzi *et al.* 2001; Perski and Jura 2003; Raucoules *et al.* 2003; Cavalié *et al.* 2008; Engelbrecht *et al.* 2011; Dong *et al.* 2013; Gupta *et al.* 2014; Przyłucka *et al.* 2015; Qin and Perissin 2015; Chatterjee *et al.* 2015, 2016; Ishwar and Kumar 2017). Earlier D-InSAR technique used the difference of phase observed by radar signals from two different acquisitions of the study area over time to detect ground deformation up to the sub-centimeter scale. However, (1) temporal and geometric decorrelation, (2) atmospheric effects, and (3) requirement of precise digital elevation model (DEM) are the main limitations of D-InSAR techniques (Zebker and Villasenor 1992; Dong *et al.* 2013). Among these three, temporal decorrelation is the leading cause of information loss at the subsidence center (Yue *et al.* 2011).

After considering the limitation of the D-InSAR technique, Ferretti *et al.* (2000) have developed the Persistent Scatterer Interferometric Synthetic Aperture Radar (PS-InSAR) technique to detect land deformation at the millimeter level. The PS-InSAR technique is the geodetic Synthetic Aperture Radar (SAR) processing technique developed in the early 1990s that uses two or more SAR images to generate maps of topography or deformation of the Earth's surface (Bamler and Hartl 1998; Massonnet and Feigl 1998; Bürgmann *et al.* 2000; Ferretti *et al.* 2001; Hanssen 2001; Kampes 2006; Simons and Rosen 2007; Prati *et al.* 2010; Hooper *et al.* 2012). Satellite-based PS-InSAR technique has shown its competence in the detection of surface height changes up to sub-millimeter precision using C-band ENVISAT ASAR data. The PS-InSAR technique reduces temporal and geometric decorrelation by selecting stable points or persistent scatterers (PSs), which is temporal and geometrically coherent in nature throughout all acquisition time-series SAR data (Crosetto *et al.* 2016). Additionally, PS-InSAR has the capability to reduce atmospheric contribution using multi-temporal time-series SAR data analysis with PSs (Ferretti *et al.* 2001; Davila-Hernandez *et al.* 2014). Perissin and Wang (2012) have developed a modified PS-InSAR (PSI) approach in which partially

correlated scatterers are also included along with permanent scatterers to increase the point target density in the highly susceptible area for decorrelation.

PS-InSAR technique has been adopted in the coal-bearing area to detect land deformation using C-Band and L-Band SAR Data (Guéguen *et al.* 2009; Abdikan *et al.* 2011; 2014; Jiang *et al.* 2011; Thapa *et al.* 2016). The chances of temporal decorrelation with C-band SAR data are higher than L-band data as it is more limited to spatial and temporal baseline (Liu *et al.* 2009). However, this study emphasises to detect the slow velocity subsidence in the coal mining area. The short wavelength C-band is more suitable to detect slow velocity subsidence if the optimal baseline is maintained, whereas long-wavelength L-band can effectively detect rapid velocity subsidence (Yue *et al.* 2011; Chatterjee *et al.* 2015; Malik *et al.* 2018). Previous studies have shown that the low density of PSs points in the coal mine area is also one of the main problems with C-Band SAR data (Abdikan *et al.* 2011). Thus, the study adopted the modified PSI technique using C-band SAR data with an optimum baseline.

The objectives of this study are: (1) to show the feasibility and credibility of modified PSI technique with C-band SAR data to detect potential slow rated subsidence in vegetated and rural areas of JCF, (2) multi-temporal analysis of 19 images of C-band ENVISAT ASAR by modified PSI through SARPROZ (Sarproz 2017) software during the long-time period (17 March 2007–10 April 2010) for land deformation monitoring and assessment over Jharia coalfield. Five major sites have been addressed with slow rate subsidence by PS-InSAR analysis over the study area. The subsidence profile generated through the present study was correlated with the master plan of JCF, showing subsidence locations (BCCL 2008).

## 2. Materials and methods

### 2.1 Study area

JCF is the largest coking coal producer in India with an area of approximately 450 km<sup>2</sup> containing various underground and open cast mines. It is a sickle shaped Gondwana coalfield occurring in the form of a basin truncated with a major boundary fault on the southern flank. Technically, Gondwana coalfield basin was formed by the

down-faulting of the crystalline basement floor, boundaries of which are marked by high angle normal faults of enechelon type. The general stratigraphic succession of the area is that the basement of metamorphic rocks is overlain by the Talcher Formation followed by the Barakar Formation which is the main coal bearing horizon. Barren measures come above Barakar Formation which is followed by the coal-bearing Raniganj Formation. The Raniganj Formation is the uppermost coal bearing formation in the JCF. It is situated in the heart of Damodar river valley towards the north-west of Kolkata at about 250 km distance and about 1150 km southeast of Delhi. In this study, a part of JCF which is confined between latitudes 23°42'00"–23°48'30"N and longitude 86°19'30"–86°30'00"E is considered as a study area (figure 1).

### 2.2 Datasets and data processing

For this study, according to the availability of data for study area 19 SLC images of ENVISAT ASAR covering the study area during the period of March 17, 2007–April 10, 2010 are downloaded from European Space Agency website. By considering scene acquired on 6th of December, 2008 as a master, the spatial and temporal baseline for the selected interferometry stack, are calculated and given in table 1. The graph plotted between spatial and temporal baseline is shown in figure 2. In this figure, the position of each slave image corresponding to master image in spatial-temporal baseline space is depicted by dots. The master date is selected considering that no precipitation would have happened on that day. The overall distribution of the baseline looks good from the perspective of interferometry stacking and only two images are found, having the spatial baseline more than 300 m.

The spatial and temporal baselines are the important factors in choosing a suitable data pair for deformation analysis. The spatial baseline is the distance between the orbits of two SAR acquisitions, whereas, temporal baseline refers to the time difference (in days) between two SAR acquisitions. Depending upon the application and the spatial resolution of the data, the appropriate spatial and temporal baseline configuration can be preferred. In this study, PS-InSAR approach was incorporated to investigate the deformation of various regimes in JCF using multi-temporal SLC images



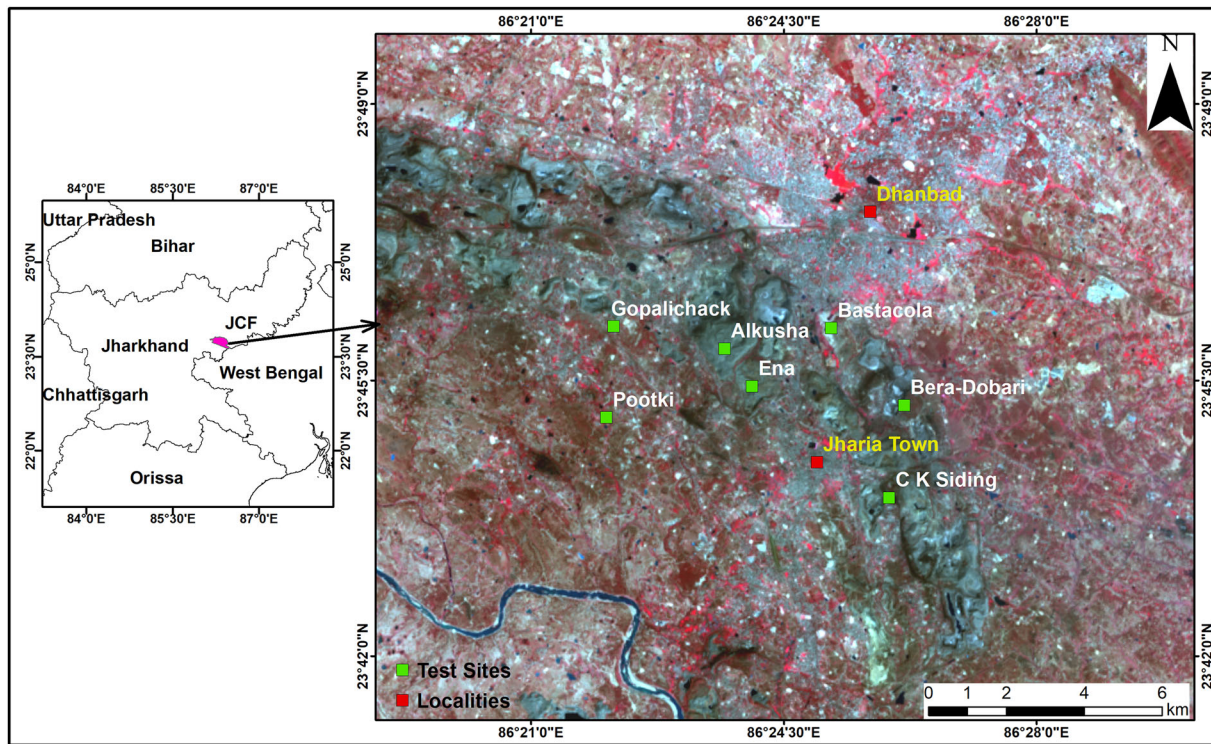


Figure 1. Location map of study area with test sites in JCF as seen in Landsat-8 OLI standard FCC image.

Table 1. *ENVISAT* images with spatial and temporal baseline.

Sl. no.	Date	Spatial baseline (m)	Temporal baseline (days)
1	17 March 2007	-335	630
2	21 April 2007	-74	595
3	26 May 2007	-31	560
4	04 August 2007	47	490
5	08 September 2007	-135	455
6	13 October 2007	106	420
7	01 March 2008	228	280
8	14 June 2008	198	175
9	27 September 2008	81	70
<b>10</b>	<b>06 December 2008</b>	<b>00</b>	<b>00</b>
11	10 January 2009	-46	35
12	14 February 2009	-144	70
13	08 August 2009	29	245
14	12 September 2009	364	280
15	17 October 2009	182	315
16	21 November 2009	-299	350
17	26 December 2009	40	385
18	30 January 2010	-288	420
19	10 April 2010	-193	490

of ENVISAT ASAR with maximum spatial and temporal baseline of 364 m and 630 days, respectively. Two-pass PS-InSAR method is used to perform the target point based analysis which

has been accomplished in SARPROZ interferometric processor and developed in MATLAB<sup>®</sup>. SARPROZ is capable in processing long time series data with different DInSAR approaches (Perissin and Wang 2012; Ruiz-Armenteros *et al.* 2016). The method has the ability to find deformation over those areas where the coherent targets (i.e., PSs) throughout the whole study time period are very few due to the decorrelation occurred in the study area. A graphical representation of the processing steps adopted in PS-InSAR processing on SARPROZ software is shown in figure 3.

The SLC images are brought into the SARPROZ software environment and a subset area for JCF region is extracted for this study. In this study, single reference scheme is considered to generate the stack of interferograms, in which the SLC image of date December 6, 2008 is taken as the master image. The slave SLC images are co-registered with the reference to the selected master image. More than 2000 tie points in the co-registration process are used to ensure sub-pixel co-registration accuracy. The possible numbers of interferograms are generated and Boxcar filter is applied on each interferogram to suppress the noise. This filter is used because of its efficiency to detect the subsidence fringes in homogenous areas (Chao *et al.* 2013). A boxcar filter has the potential

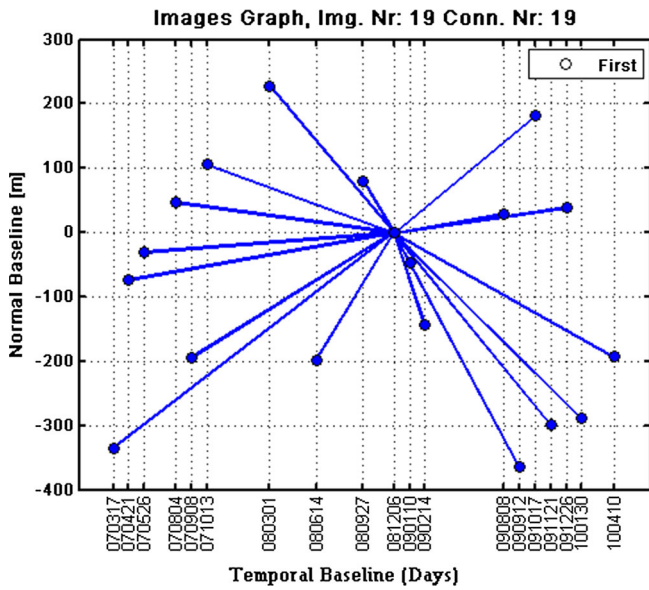


Figure 2. Spatial and temporal baseline graph.

to compute the output image pixel as an equal weighting of a neighborhood of pixels of the corresponding input image pixel. It is comparatively better than other low pass filter. In APS processing, a network of PS targets is formed by applying a threshold of 0.70 on ASI to acquire the initial parameters and estimate APS. Thereafter, reflectivity map, amplitude stability indices (ASI), and temporal and spatial coherence are calculated for each radar image. The Shuttle Radar Topography Mission (SRTM) DEM is used with ground resolution 3 arcsec (90 m) to remove the topography from interferogram and to generate the differential interferograms. It is also used for flattening and geocoding of interferograms. In atmospheric phase screen (APS) processing, a network of PS targets is formed by applying a threshold of 0.70 on ASI to estimate the initial parameters and APS. The

formula used in the calculation of ASI is given as follows:

$$ASI = 1 - \frac{\sigma_A}{m_A}, \tag{1}$$

where  $m_A$  and  $\sigma_A$  are the mean and the standard deviation of the amplitude values, respectively.

The estimated APS is removed from the differential interferograms to reduce the atmospheric phase delay contribution. After APS removal, the final step of SPS processing is carried out which is applied on the PSs network to get the final estimation of height and line of sight (LOS) velocity for the generation of cumulative displacement map over the PS points (Perissin and Wang 2012).

### 3. Results and discussion

The 19 SLC images with the master image (December 6, 2008) were used to generate 18 interferograms using modified PS-InSAR approach through SARPROZ software. After analyzing these 19 SLC images, the maximum perpendicular and temporal baseline were found to be 364 m and 630 days, respectively, while the minimum perpendicular baseline is 29 m, and the temporal baseline is 35 days. The PSs were selected on the basis of the ASI threshold value of 0.70, which signifies the stability of target points. The lower value of ASI observations for a target indicates low stability of the ground. This threshold value of ASI was picked to get a sufficient number of stable targets in the study area. The LOS displacement was improved by using APS and atmospheric phase delay correction. Later, the LOS displacement velocity on PS locations was

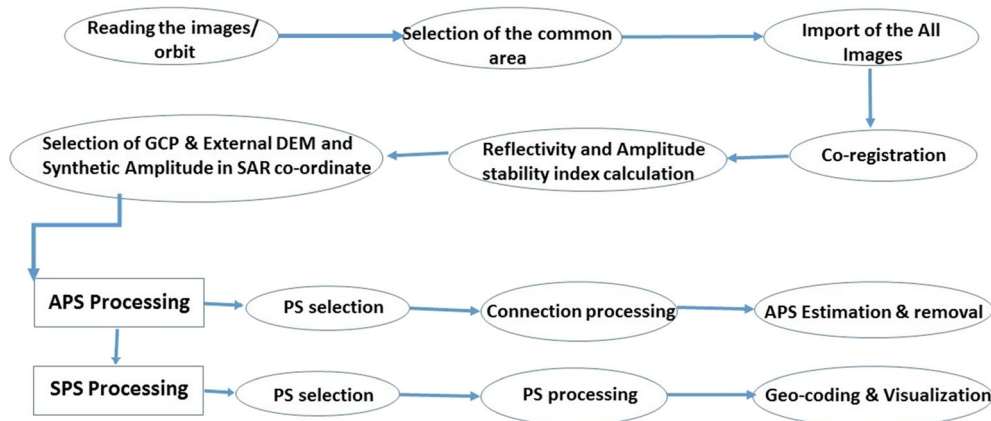


Figure 3. Flow chart of PS-InSAR processing on SARPROZ software.

estimated. The results showed that there is an occurrence of subsidence in all the five locations of JCF viz., Alkusha, Ena, Bastacola, Bera–Dobari, and CK-Siding. The sites are non-urban areas and highly sensitive for temporal change of surface features. Therefore, less number of PS points for the above-mentioned threshold was observed over the test sites. Around each test site, a buffer zone was created. Those number of PS points which matched the threshold value of ASI and belonged to the buffer zone of the test site were considered for the estimation of subsidence rate during the whole study period of 3 yrs and 1 month (figure 4). The temporal coherence of all the selected PSs was also tested. The PSs, which were having a temporal coherence value  $<0.5$ , have been discarded from further processing. The PS points having ASI value of 0.7 and above, and temporal coherence of 0.5 and above, gave a relatively stable estimation of LOS velocity. The following results of various locations of the study area are summarized in terms of yearly subsidence (i.e., subsidence rate (mm/year)).

Alkusha is under area VIII of BCCL. Here 10 PS points were considered out of which four PSs were showing cumulative subsidence around 90 mm during the whole study period with an yearly rate of subsidence amounting to 27 mm/yr (figure 5a). The occurrence of the subsidence has also been reported by the BCCL Master Plan (BCCL 2008) during the study period. In this region, seams XIV, XIII, XII and XI are affected by the fire and declared as a subsidence prone area. Some schemes such as blind flushing and surface sealing have been adopted by mine authority to control fire and fire-induced land subsidence. Figure 6(a) illustrates the influence of land subsidence habitant area near Alkusha colliery. Thus the land subsidence results for the Alkusha site obtained from SAR data analysis are correlated with documented results by BCCL.

Ena falls under area VIII of BCCL. In this area, 10 PSs were identified (figure 4c). Each PS showed a different rate of subsidence. The fastest moving point was showing an yearly subsidence rate of 28 mm/year (figure 5b), while the slowest one was

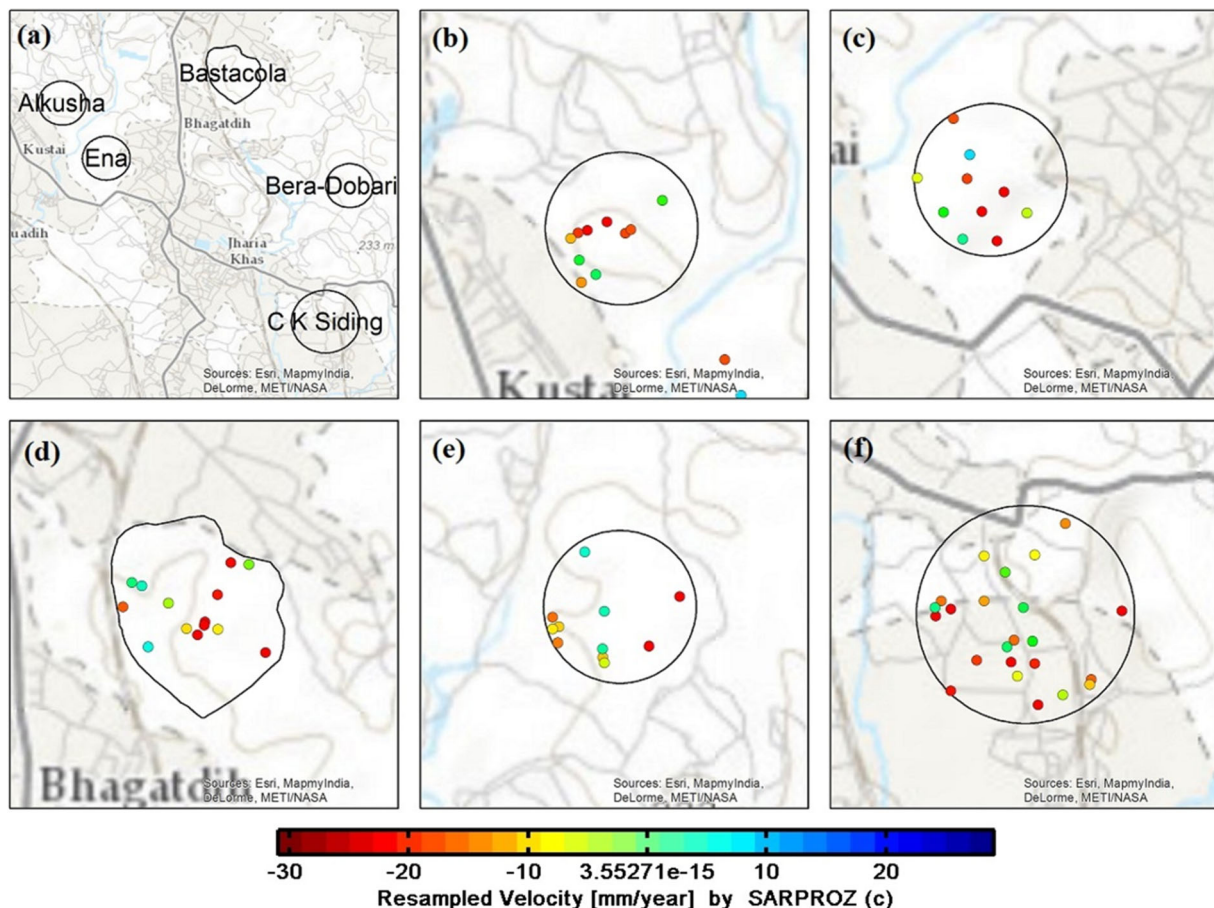


Figure 4. Selected PS points over test sites in JCF (a) composite sites, (b) Alkusha, (c) Ena, (d) Bastacola, (e) Bera-Dobari, and (f) CK-siding.



showing a subsidence rate of 10 mm/year. This area is also affected by fire in seam XIV and seam XV, which is one of the important causes of subsidence. Visual subsidence has been reported in this region as per BCCL master plan (BCCL 2008). The report has also recommended various schemes to deal with the coal fire (e.g., trench excavation and soil filing) and subsidence (e.g., blind flushing and surface sealing) at Ena colliery.

Bastacola is located on the east side of Dhanbad–Sindri road under area IX of BCCL, as shown in figure 4(d). In this region, coal seam III has been depillared by Bord and Pillar method. In Bord and Pillar method of coal extraction, coal pillars are formed as natural support in mines. Six PSs were found to exhibit subsidence among the significant number of PSs in this area. The average subsidence

rate of 6 PSs is around 10 mm/yr, and another 10 PSs of the area signifies a very slow rate of subsidence which might be due to the Bord and Pillar working method in this vicinity.

Bera–Dobari as illustrated in figure 4(e) belongs to area IX of BCCL. Fourteen numbers of PSs were observed in this region with varying subsidence rates. Some PSs were found to show a high rate of subsidence (28 mm/year), with the cumulative displacement of 87 mm and remaining PSs appear almost stable. Various seams such as seam numbers X, VIII, VII, VI, and V are affected by a coal fire, as mentioned in the master plan (BCCL 2008), which is the major factor of subsidence in this area. The pervious study confirmed the land subsidence in Bera–Dobari with the help of DInSAR technique (Chattrejee *et al.* 2015). Cracks and local

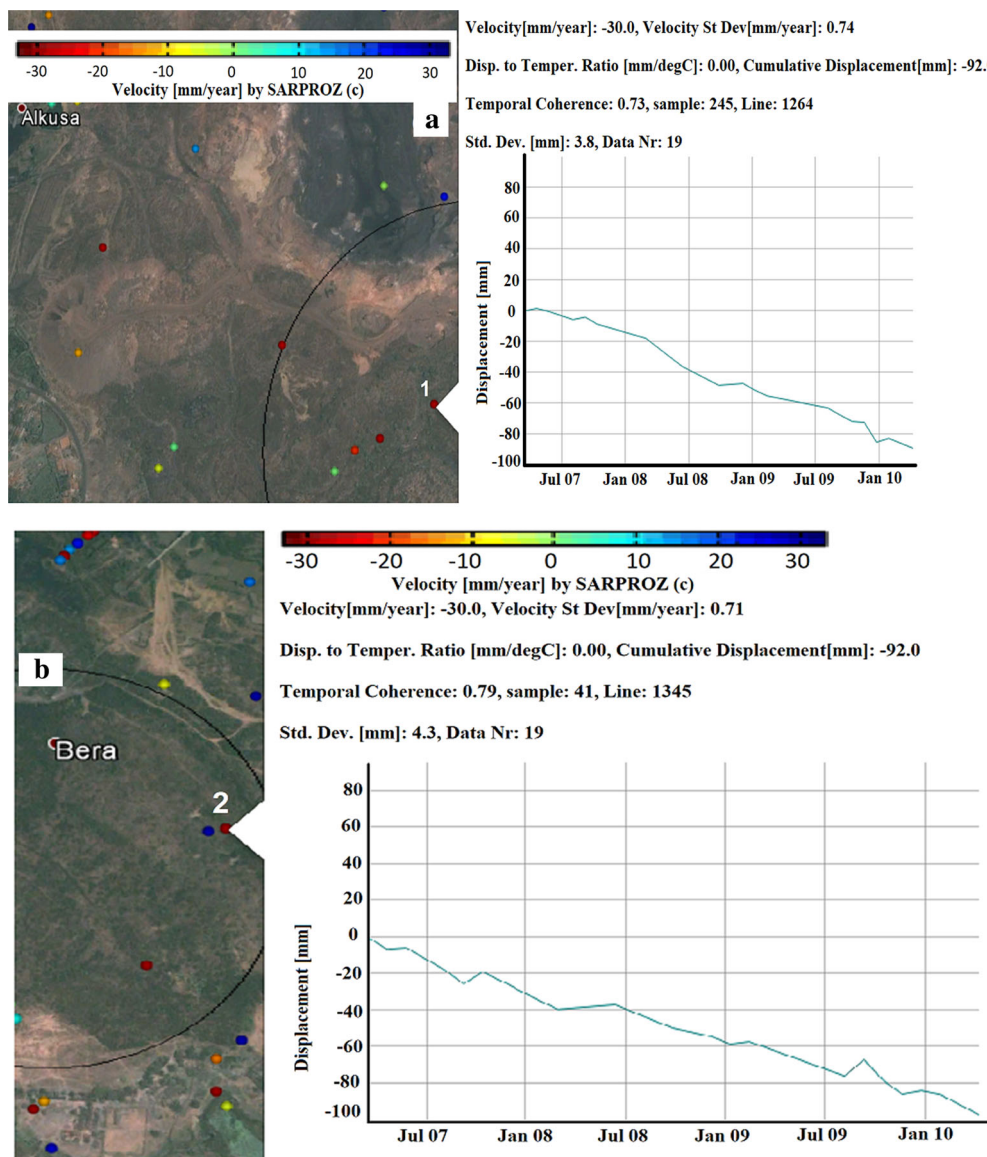


Figure 5. Estimated LOS subsidence at (a) PS point 1 (Alkusha area) and (b) PS point 2 (Bera area).

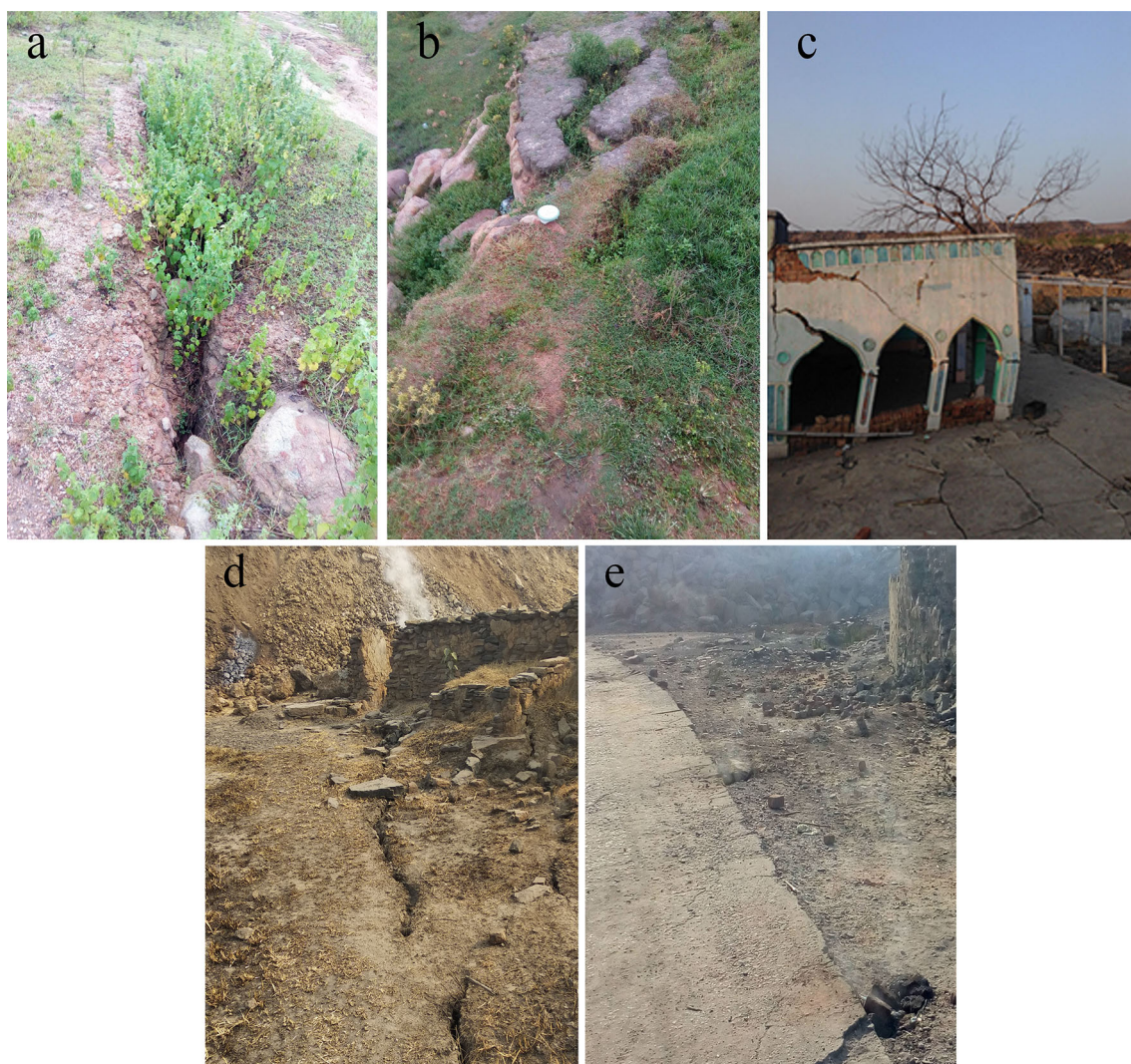


Figure 6. Visualization of subsidence in the study area (a) cracks developed, (b) subsidence occurred, (c) damaged building, (d) Bera-Dobari, and (e) CK-siding.

subsidence reported during the time span also support the results obtained by PS-InSAR technique (figure 6d).

CK-Siding is located near Ghanuadih under area IX of BCCL, which is shown in figure 4(f). This region also contains the appropriate number of PSs with mostly showing subsidence rate in between 10 and 21 mm/yr, whereas, few points are practically stable. A significant number of permanent features were observed in this area, such as residential houses and railways tracks for wagon loading. So, large numbers of PSs were noticed in this vicinity. It was also found that this area was less affected by mining excavation, which might be responsible for low subsidence rate than other test sites except for Bastacola test site. Figure 6(e) depicts the subsidence affected zone under CK-Siding.

#### 4. Conclusions

In the present study, slow land deformation in JCF due to underground activity and subsurface fire has been explored from multi-temporal C-band ENVISAT ASAR data by modified PS-InSAR technique. The adopted technique with C-band SAR data has shown its capability to witness slow subsidence from coherent targets as well as partially coherent targets in vegetated and rural areas such as Alkusha, Ena, Bastacola, Bera–Dobari, and CK-Siding of JCF. From the obtained results, it is evident that the studied area is undergoing a significant rate of subsidence mainly due to the underground mine activity as well as subsurface coal fire on coal seams. Few sites, as identified in the study area, are severely affected by subsidence. Alkusa site is showing a higher rate of subsidence,



close to 29 mm/yr, and cumulative subsidence of 90 mm. The subsidence profile generated for the above-mentioned sites in JCF was substantiated by the visual observations as well as BCCL master plan reporting subsidence locations. Hence it may be concluded that the modified PS-InSAR technique has good potential to detect land subsidence in Jharia coalfield having adverse land use land covers (vegetated and rural areas).

It is further concluded that the multi-temporal analysis of C-band SAR data with adopted methodology is practically feasible for detection, monitoring, and mapping of the slow rate of surface subsidence in coal mine areas. However, the accuracy of the subsidence rate estimation can be significantly improved by analyzing more number of images with the extended time period of observations.

## Acknowledgements

The authors would like to extend warm thanks to Dr. Daniele Perissin for providing access to SAR-PROZ software for this research study. The authors convey sincere thanks to the officials of the Department of Environment and Department of Surveying, Bharat Coking Coal Limited, Dhanbad (India), for providing supports during the field studies.

## References

- Abdikan S, Arikian M, Sanli F B and Cakir Z 2014 Monitoring of coal mining subsidence in peri-urban area of Zonguldak city (NW Turkey) with persistent scatterer interferometry using ALOS-PALSAR; *Environ. Earth Sci.* **71** 4081–4089.
- Abdikan S, Hooper A, Arikian M, Balik Sanli F, Cakir Z and Kemalderer H 2011 InSAR time series analysis of coal mining in Zonguldak city, Northwestern Turkey; In: *Fringe Workshop*.
- Bamler R and Hartl P 1998 Synthetic aperture radar interferometry; *Inverse Probl.* **14** R1.
- BCCL 2008 Master Plan for dealing with fire, subsidence and rehabilitation in the lease hold of BCCL; <http://www.bcclweb.in/PDFs/MPLANBCCL-2008.pdf>.
- Bürgmann R, Rosen P A and Fielding E J 2000 Synthetic aperture radar interferometry to measure Earth's surface topography and its deformation; *Ann. Rev. Earth Planet. Sci.* **28** 169–209.
- Carnec C and Delacourt C 2000 Three years of mining subsidence monitored by SAR interferometry, near Gardanne, France; *J. Appl. Geophys.* **43** 43–54.
- Cavalié O, Lasserre C, Doin M-P, Peltzer G, Sun J, Xu X and Shen Z-K 2008 Measurement of interseismic strain across the Haiyuan fault (Gansu, China), by InSAR; *Earth Planet. Sci. Lett.* **275** 246–257.
- Chao C-F, Chen K-S and Lee J-S 2013 Refined filtering of interferometric phase from InSAR data; *IEEE Trans. Geosci. Remote Sens.* **51** 5315–5323.
- Chatterjee R S 2006 Coal fire mapping from satellite thermal IR data – a case example in Jharia Coalfield, Jharkhand, India; *ISPRS J. Photogramm. Remote Sens.* **60** 113–128.
- Chatterjee R S, Fruneau B, Rudant J P, Roy P S, Frison P-L, Lakhera R C, Dadhwal V K and Saha R 2006 Subsidence of Kolkata (Calcutta) City, India during the 1990s as observed from space by differential synthetic aperture radar interferometry (D-InSAR) technique; *Remote Sens. Environ.* **102** 176–185.
- Chatterjee R S, Singh K B, Thapa S and Kumar D 2016 The present status of subsiding land vulnerable to roof collapse in the Jharia Coalfield, India, as obtained from shorter temporal baseline C-band DInSAR by smaller spatial subset unwrapped phase profiling; *Int. J. Remote Sens.* **37** 176–190.
- Chatterjee R S, Thapa S, Singh K B, Varunakumar G and Raju E V R 2015 Detecting, mapping and monitoring of land subsidence in Jharia Coalfield, Jharkhand, India by spaceborne differential interferometric SAR, GPS and precision levelling techniques; *J. Earth Syst. Sci.* **124** 1359–1376.
- Crosetto M, Monserrat O, Cuevas-González M, Devanthéry N and Crippa B 2016 Persistent scatterer interferometry: A review; *ISPRS J. Photogramm. Remote Sens.* **115** 78–89.
- Davila-Hernandez N, Madrigal D, Exposito J L and Antonio X 2014 Multi-temporal analysis of land subsidence in Toluca Valley (Mexico) through a combination of Persistent Scatterer Interferometry (PSI) and historical piezometric data; *Adv. Remote Sens.* **3** 49.
- Dong S, Yin H, Yao S and Zhang F 2013 Detecting surface subsidence in coal mining area based on DInSAR technique; *J. Earth Syst. Sci.* **24** 449–456.
- Engelbrecht J and Inggis M 2013 Differential interferometry techniques on L-band data employed for the monitoring of surface subsidence due to mining; *South African J. Geomatics* **2** 82–93.
- Engelbrecht J, Inggis M R and Makusha G 2011 Detection and monitoring of surface subsidence associated with mining activities in the Witbank Coalfields, South Africa, using differential radar interferometry; *South African J. Geol.* **114** 77–94.
- Ferretti A, Prati C and Rocca F 2000 Nonlinear subsidence rate estimation using permanent scatterers in differential SAR interferometry; *IEEE Trans. Geosci. Remote Sens.* **38**(5) 2202–2212.
- Ferretti A, Prati C and Rocca F 2001 Permanent scatterers in SAR interferometry; *IEEE Trans. Geosci. Remote Sens.* **39** 8–20.
- Guang L, Huadong G, Xiaofang G, Perski Z and Huanyin Y 2009 Mining area subsidence monitoring using multi-band SAR data; In: *Urban Remote Sensing Event*, pp. 1–6.
- Guéguen Y, Deffontaines B, Fruneau B, Al Heib M, De Michele M, Raucoules D, Guise Y and Planchenault J 2009 Monitoring residual mining subsidence of Nord/Pas-de-Calais coal basin from differential and Persistent Scatterer Interferometry (Northern France); *J. Appl. Geophys.* **69** 24–34.
- Gupta M, Mohanty K K, Kumar D and Banerjee R 2014 Monitoring surface elevation changes in Jharia coalfield,

- India using synthetic aperture radar interferometry; *Environ. Earth Sci.* **71** 2875–2883.
- Hanssen R F 2001 *Radar Interferometry: Data Interpretation and Error Analysis*; Springer Science & Business Media, Berlin.
- Hooper A, Bekaert D, Spaans K and Arikan M 2012 Recent advances in SAR interferometry time series analysis for measuring crustal deformation; *Tectonophysics*. **514** 1–13.
- Ishwar S G and Kumar D 2017 Application of DInSAR in mine surface subsidence monitoring and prediction; *Curr. Sci.* **112** 46–51.
- Jiang L, Lin H, Ma J, Kong Band Wang Y 2011 Potential of small-baseline SAR interferometry for monitoring land subsidence related to underground coal fires: Wuda (Northern China) case study; *Remote Sens. Environ.* **115** 257–268.
- Jianjun S, Chunjian H, Ping L, Junwei Z, Deyuan L, Minde J, Lin Z, Jingkai Z and Jianying S 2012 Quantitative prediction of mining subsidence and its impact on the environment; *Int. J. Min. Sci. Technol.* **22** 69–73.
- Jing-xiang G and Hong H 2009 Advanced GNSS technology of mining deformation monitoring; *Proc. Earth Planet. Sci.* **1** 1081–1088.
- Kampes B M 2006 *Radar interferometry*; Springer.
- Liu G, Buckley S M, Ding X, Chen Q and Luo X 2009 Estimating spatiotemporal ground deformation with improved persistent-scatterer radar interferometry; *IEEE Trans. Geosci. Remote Sens.* **47**(9) 3209–3219.
- Lü W-C, Cheng S-G, Yang H-S and Liu D-P 2008 Application of GPS technology to build a mine-subsidence observation station; *J. China Univ. Min. Technol.* **18** 377–380.
- Malik K, Kumar D and Perissin D 2018 Assessment of subsidence in Delhi NCR due to groundwater depletion using TerraSAR-X and persistent scatterers interferometry; *Imag. Sci. J.* **67** 1–7, <https://doi.org/10.1080/13682199.2018.1540166>.
- Massonnet D and Feigl K L 1998 Radar interferometry and its application to changes in the Earth's surface; *Rev. Geophys.* **36** 441–500.
- Miao F, Yan M, Qi X, Ye C, Wang B, Liu R and Chen J 2008 Application of DInSAR and GIS for underground mine subsidence monitoring; *Int. Arch. Photogramm. Remote Sens. Spat. Inf. Sci.* **37** 251–256.
- Mukherjee T K, Bandyopadhyay T K and Pande S K 1991 Detection and delineation of depth of subsurface coalmine fires based on an airborne multispectral scanner survey in a part of the Jharia Coalfield, India; *Photogramm. Eng. Remote Sens.* **57**(9) 1203–1207.
- Pandey J, Kumar D, Singh V K and Mohalik N K 2016 Environmental and socio-economic impacts of fire in Jharia Coalfield, Jharkhand, India: An appraisal; *Curr. Sci.* **110** 1639–1650.
- Paradella W R, Ferretti A, Mura J C, Colombo D, Gama F F, Tamburini A, Santos A R, Novali F, Galo M and Camargo P O 2015 Mapping surface deformation in open pit iron mines of Carajás Province (Amazon Region) using an integrated SAR analysis; *Eng. Geol.* **193** 61–78.
- Perissin D and Wang T 2012 Repeat-pass SAR interferometry with partially coherent targets; *IEEE Trans. Geosci. Remote Sens.* **50** 271–280.
- Perski Z 1998 Applicability of ERS-1 and ERS-2 InSAR for land subsidence monitoring in the Silesian coal mining region, Poland; *Int. Arch. Photogramm. Remote Sens.* **32** 555–558.
- Perski Z and Jura D 2003 Identification and measurement of mining subsidence with SAR interferometry: Potentials and limitations; In: Proceedings, 11th FIG symposium on deformation measurements, Santorini, Greece.
- Prati C, Ferretti A and Perissin D 2010 Recent advances on surface ground deformation measurement by means of repeated space-borne SAR observations; *J. Geodyn.* **49** 161–170.
- Przyłucka M, Herrera G, Graniczny M, Colombo D and Béjar-Pizarro M 2015 Combination of conventional and advanced DInSAR to monitor very fast mining subsidence with TerraSAR-X Data: Bytom City (Poland); *Remote Sens.* **7** 5300–5328.
- Qin Y and Perissin D 2015 Monitoring underground mining subsidence in South Indiana with C- and L-band InSAR technique; In: *IEEE International on Geoscience and Remote Sensing Symposium (IGARSS)*, pp. 294–297.
- Raucoules D, Maisons C, Carnec C, Le Mouelic S, King C and Hosford S 2003 Monitoring of slow ground deformation by ERS radar interferometry on the Vauvert salt mine (France): Comparison with ground-based measurement; *Remote Sens. Environ.* **88** 468–478.
- Ruiz-Armenteros A M, Bakon M, Lazecky M, Delgado J M, Sousa J J, Perissin D and Caro-Cuenca M 2016 Multi-temporal InSAR processing comparison in presence of high topography; *Procedia Comput. Sci.* **100** 1181–1190.
- Sarproz 2017 <https://www.sarproz.com/>.
- Shen B and Poulsen B 2014 Investigation of overburden behaviour for grout injection to control mine subsidence; *Int. J. Min. Sci. Technol.* **24** 317–323.
- Simons M and Rosen P A 2007 Interferometric synthetic aperture radar geodesy; In: *Treatise on Geophysics, Geodesy*, Elsevier, Amsterdam, vol. 3, pp. 391–446.
- Stow R J and Wright P 1997 Mining subsidence land survey by SAR interferometry; In: *Third ERS Symposium on Space at the Service of Our Environment*, 525p.
- Strozzi T, Wegmuller U, Tosi L, Bitelli G and Spreckels V 2001 Land subsidence monitoring with differential SAR interferometry; *Photogramm. Eng. Remote Sens.* **67** 1261–1270.
- Thapa S, Chatterjee R S, Singh K B and Kumar D 2016 Land subsidence monitoring using PS-InSAR technique for l-band SAR data; *ISPRS – Int. Arch. Photogramm. Remote Sens. Spat. Info. Sci.*, <https://doi.org/10.5194/isprs-archives-xli-b7-995-2016>.
- Wang J, Peng X and Xu C H 2011 Coal mining GPS subsidence monitoring technology and its application; *Min. Sci. Technol.* **21** 463–467, <https://doi.org/10.1016/j.mstc.2011.06.001>.
- Yue H, Liu G, Perski Z and Guo H 2011 Satellite radar reveals land subsidence over coal mines; *SPIE Newsroom*, **3**.
- Zebker H A and Villasenor J 1992 Decorrelation in interferometric radar echoes; *IEEE Trans. Geosci. Remote Sens.* **30** 950–959, <https://doi.org/10.1109/36.175330>.